arXiv:2301.01054v2 [eess.IV] 6 Jul 2023

BENCHMARKING COMMON UNCERTAINTY ESTIMATION METHODS WITH HISTOPATHOLOGICAL IMAGES UNDER DOMAIN SHIFT AND LABEL NOISE

PREPRINT

Hendrik Mehrtens[1], **Alexander Kurz**[1], **Tabea-Clara Bucher, Titus J. Brinker**[2]
Division of Digital Biomarkers for Oncology
German Cancer Research Center (DKFZ)
Heidelberg, Germany
{hendrikalexander.mehrtens},{alexander.kurz},{tabea.bucher}@dkfz-heidelberg.de
titus.brinker@nct-heidelberg.de

September 2022

ABSTRACT

In the past years, deep learning has seen an increase in usage in the domain of histopathological applications. However, while these approaches have shown great potential, in high-risk environments deep learning models need to be able to judge their uncertainty and be able to reject inputs when there is a significant chance of misclassification. In this work, we conduct a rigorous evaluation of the most commonly used uncertainty and robustness methods for the classification of Whole Slide Images, with a focus on the task of selective classification, where the model should reject the classification in situations in which it is uncertain. We conduct our experiments on tile-level under the aspects of domain shift and label noise, as well as on slide-level. In our experiments, we compare Deep Ensembles, Monte-Carlo Dropout, Stochastic Variational Inference, Test-Time Data Augmentation as well as ensembles of the latter approaches. We observe that ensembles of methods generally lead to better uncertainty estimates as well as an increased robustness towards domain shifts and label noise, while contrary to results from classical computer vision benchmarks no systematic gain of the other methods can be shown. Across methods, a rejection of the most uncertain samples reliably leads to a significant increase in classification accuracy on both in-distribution as well as out-of-distribution data. Furthermore, we conduct experiments comparing these methods under varying conditions of label noise. Lastly, we publish our code framework to facilitate further research on uncertainty estimation on histopathological data.

Keywords Deep learning, Uncertainty estimation, Robustness, Histopathology, Domain shift, Label noise

1 Introduction

Deep Neural Networks (DNNs) have been shown to be of equal or even superior performance in studies on many medical tasks [Esteva et al., 2017, Haenssle et al., 2018, Hekler et al., 2019], compared to human practitioners. Nonetheless, they have rarely been adopted in clinical practice. One commonly given reason [Begoli et al., 2019, Kompa et al., 2021, van der Laak et al., 2021] is their inability to provide well-calibrated estimates of their predictive uncertainty [Guo et al., 2017], thereby prohibiting the practitioner from judging the reliability of the system's decision, which is a necessary condition in areas of high uncertainty like medical decision-making.

Ideally, a well-calibrated deep learning system should be able to judge and communicate a correct estimate of its certainty in each prediction, not only informing the human practitioner of its momentary reliability but also enabling

[1]Contributed equally
[2]Corresponding author

the system to automatically reject inputs [Band et al., 2021, Jaeger et al., 2023] and refer them to humans for inspection, thereby enhancing the reliability of the system.

Another problem in practice is the high vulnerability of DNN-based systems to "domain shifts", which are differences between the data distributions in the training and deployment setting. In the general machine learning literature, [Hendrycks and Dietterich, 2019, Ovadia et al., 2019] noticed the vulnerability of deep neural networks to even slight artificial perturbations of images, which result in drastic deterioration of classification performance. In the area of digital pathology, these kinds of shifts are very common [Stacke et al., 2021]. They arise due to different data-acquisition processes across clinics, for example, due to different staining procedures or different scanners but can also be caused by changes in the distribution of patient characteristics (gender, age, etc.). The unpredictable behavior of models in new data regimes limits the ability to put confidence in a system's decision, especially in high-risk environments, an example being decisions that affect a patient's treatment.

Traditional methods for improving the generalization of a machine learning system use augmentations of the input data, which is currently heavily investigated in the field of digital histopathology [Tellez et al., 2019]. In recent years, several new techniques for uncertainty quantification and generalization under domain shift have been proposed. Yet, most of these methods have primarily been evaluated in the general setting of computer vision and object detection, with limited research on them specifically in the field of digital pathology.

Whole Slide Images (WSIs) are a challenging domain for deep learning, due to the large size of the images, typically at the gigapixel scale, and the limited availability of labeled data. Additionally, as the evaluation of a WSI is error-prone, with high inter-observer variability [Karimi et al., 2020], labels can be subject to a high degree of label noise, making the integration of predictive certainty vital.

[Linmans et al., 2020] explored the capability of multi-headed ensemble networks to detect out-of-distribution (OOD) inputs in WSIs. [Thagaard et al., 2020] compared the ability of Deep Ensembles [Lakshminarayanan et al., 2017] and Monte-Carlo Dropout (MCDO) [Gal and Ghahramani, 2016] to estimate predictive uncertainty at the tile-level. Independently and concurrent to our work, [Linmans et al., 2023] compared prominent methods for uncertainty estimation on histopathological slides, with a focus on out-of-distribution detection of foreign tissue in breast and prostate tissues. Building upon Jaeger's [Jaeger et al., 2023] insights on meaningful and comparable evaluation of uncertainty estimation methods, we investigate the ability of uncertainty estimation methods to reject uncertain predictions. Our evaluations are performed at the tile-level, as well as at the slide-level, which is the clinically more relevant task.

We carefully compare the robustness of Deep Ensembles [Lakshminarayanan et al., 2017], MCDO [Gal and Ghahramani, 2016], Stochastic Variational Inference (SVI) [Blundell et al., 2015], Test-Time Data Augmentation (TTA) [Ayhan and Berens, 2018] and ensembles of the latter approaches under domain shift. We study the impact of the reject option by uncertainty on the performance of the model, observing a significant increase in accuracy in high-certainty predictions, and compare multiple metrics of estimating the final certainty from the predictions. We simulate the effects of label noise in the edge regions of the tumor annotations and measure the robustness of the methods to this induced label noise.

For our experiments, we use multiple tumorous histopathological datasets. For our tile-level experiments, we utilize the Camelyon17 [Bándi et al., 2019] dataset. The Camelyon17 breast cancer tissue dataset comprises a total of 50 slides with annotated tumor regions. These slides were obtained in five different clinics, using three different scanners, enabling the evaluation of different approaches in a realistic domain shift scenario.

In our slide-level experiments, we utilize tissue slides from The Cancer Genome Atlas (TCGA). The molecular characteristics of the dataset were evaluated in [Liu et al., 2018], providing mutation status information such as Microsatellite Instability (MSI) for each sample. Considering the clinically relevant task of making predictions directly from whole tissue slides, we apply uncertainty estimation to the task of MSI prediction from WSIs in the TCGA colorectal dataset.

Our main contributions are:

- A detailed analysis of the extent to which rejecting uncertain samples enhances classification performance on both tile and slide-level.
- A systematic comparison of the most prominent uncertainty estimation methods under domain shift in terms of selective classification, network calibration, and classifier performance on histopathological data.
- An investigation of the influence of label noise on the classification of WSIs and the robustness of the included uncertainty estimation methods against it.

- The release of an easily extendable code repository[1] to facilitate further research on uncertainty estimation for deep neural networks.

2 Methods

In this section, we describe the methods, uncertainty measures and evaluation settings used in our work.

2.1 Uncertainty Estimation Methods

In uncertainty estimation, we want to compute the posterior predictive distribution of the output $\mathbf{y}$, given an input $\mathbf{x}$ and training data $\mathcal{D}$. This distribution can be formulated using Bayesian Model Averaging over the model's parameters $\mathbf{w}$ as

$$p(\mathbf{y}|\mathbf{x}, \mathcal{D}) = \int p(\mathbf{y}|\mathbf{x}, \mathbf{w}) p(\mathbf{w}|\mathcal{D}) \, \mathrm{d}\mathbf{w} \tag{1}$$

However, the posterior predictive distribution for neural networks is analytically intractable. As a result, in recent years several approximation methods have been proposed. Other methods are not motivated by Bayesian statistics but are nonetheless commonly used for quantifying predictive uncertainty. In the following, we briefly introduce the most prominent methods.

Stochastic Variational Inference (SVI): [Blundell et al., 2015] and [Graves, 2011] approximate the posterior distribution by placing a Gaussian distribution over every parameter of the neural network. As an objective for the approximation, the estimated lower-bound (ELBO) is minimized [Blei et al., 2017]. We use the Flipout formulation [Wen et al., 2018] of SVI for stabilizing the training procedure.

Monte-Carlo Dropout (MCDO): [Gal and Ghahramani, 2016] show that the dropout operation, originally intended as a regularization method to stabilize neural network training, can be used to approximate the true posterior of the neural network. For the approximation, multiple forward passes of the same input, with activated dropout layers, are aggregated during inference. The distribution over the predictions obtained through this method can be seen as samples from an approximation of the posterior distribution.

Deep Ensemble: A Deep Ensemble [Lakshminarayanan et al., 2017] consists of multiple, in architecture identical, neural networks that are trained from different random initializations. The mean of all ensemble members serves as the prediction during inference. [Ovadia et al., 2019, Ashukha et al., 2020] show that Deep Ensembles outperform many other methods in terms of calibration and robustness under domain shift.

Test-Time Data Augmentations (TTA): In contrast to Deep Ensembles, which employ multiple models during inference, TTA uses the same model multiple times by augmenting the input in different ways during inference. Generally, the same augmentations as at training time are applied during inference. [Ayhan and Berens, 2018, Ashukha et al., 2020] show the good performance of TTA in terms of robustness and calibration, which can come close to the performance of a Deep Ensemble while requiring less training time, as only one model is trained.

Ensemble Variants: Additionally, ensemble variants of the methods SVI, MCDO and TTA are implemented and tested.

2.2 Uncertainty Metrics

Given the predictions generated by the previously introduced methods, the literature developed multiple metrics to estimate the predictive uncertainty.

The most commonly used approach in the field of calibration [Guo et al., 2017] is the so-called "confidence" of the prediction, which is the maximum of the softmax output. The core idea is that decisions that are far away from the decision boundary can be considered certain, while the most uncertain decisions lie close to the boundary, which is at $1/N$, where N is the number of classes. Other commonly used uncertainty metrics encompass the entropy [Mobiny et al., 2019, Band et al., 2021] of the prediction and the variance between predictions for ensemble-like outputs [Nair et al., 2020, Leibig et al., 2017]. In B we compare these approaches and conclude that the commonly used confidence measure is well-suited for this task.

[1] `https://github.com/DBO-DKFZ/uncertainty-benchmark`

2.3 Evaluation Settings

This section covers the different evaluation settings and the performance metrics used in each setting. We evaluate on tile-level with lesion-level annotations, as well as on the slide-level, where we only utilize slide-level labels.

Reject Option: In a clinical setting, the model should be able to refer predictions with high uncertainty to human practitioners for evaluation, which is called selective classification Geifman and El-Yaniv [2017]. Models suitable for this task should assign higher uncertainties to their wrong predictions than to their correct predictions, thereby allowing to cut off a large number of false predictions, by thresholding at a certainty level. To compare multiple models on this ability, we compute the accuracy-reject curve [Nadeem et al., 2009], plotting the achieved accuracy against the percentage of rejected data points in the dataset. We also compare the area under the curve of the accuracy-reject curves ($AUARC$). This evaluation has been recommended by Jaeger et al.[Jaeger et al., 2023], where different evaluation practices in the field of failure detection have been compared and evaluated.

Calibration: For measuring calibration, we utilize the Expected Calibration Error (ECE) [Guo et al., 2017, Nixon et al., 2019]. Given a prediction for every data point in the dataset, the output probability or "confidence" for each sample should on average match the correctness of the prediction. In other words, we expect a prediction that has a confidence value of 60% to be correct in about 60% of the cases. To validate this intuition, the predictions are split into a predetermined number M of bins B of equal confidence range. Then the absolute difference between the average accuracy and confidence within each bin is summed up:

$$\mathrm{ECE} = \sum_{m=1}^{M} \frac{|B_m|}{n} \Big| \mathrm{acc}(B_m) - \mathrm{conf}(B_m) \Big| \tag{2}$$

Here, $|B_m|$ denotes the number of samples in the m-th bin and n is the total number of samples.

Label Noise: Medical annotations are often subject to an unquantified amount of label noise [Joskowicz et al., 2019, Jensen et al., 2019, Karimi et al., 2020], which may deteriorate the performance of supervised machine learning approaches. To our knowledge, the previously described methods have not been compared in their robustness to label noise in the medical domain. We evaluate the effect of label noise by creating multiple datasets with increasing levels and different types of label noise and evaluate the methods under these changing conditions.

3 Experiment setup

3.1 Datasets and data processing

Camelyon17: We conduct our experiments on the lesion-level annotated slides of the Cameylon17 dataset [Bándi et al., 2019]. This part of the Camelyon17 dataset consists of 50 WSIs of breast lymph node tissue, with annotated metastatic tissue. The slides were obtained from five different clinics in the Netherlands, using three different scanners, providing an ideal setting to assess the impact of domain shift between clinics on model performance.

To induce a distribution shift between an in-distribution (ID) and an out-of-distribution (OOD) domain, we create two distinct splits of the contributing centers. The weak domain shift is based solely on location, as the out-of-distribtion (OOD) dataset contains scanners, that are also present in the in-distribution (ID) dataset. For this split, centers 0, 2, and 4 are part of the in-distribution (ID) dataset, containing the 3D Histech, Hamamatsu and Philips scanner, while centers 1 and 3 are used as OOD datasets, which both use the 3D Histech scanner.

To induce a strong domain shift, we split the centers in a manner, that the OOD datasets only contain scanners that are not present in the ID datasets, thereby creating an additional technological shift in the image acquisition process. For this, centers 0, 1 and 3 with the 3D Histech scanners are the ID datasets, with centers 2 and 4 being OOD (Philips and Hamamatsu).

For both splits, we then further partition the ID data into training, validation and test set. We sort the slides of each center based on the area of annotated tumor cells they contain and use the two median slides as the test set for each center. The training and validation sets are generated by a randomized $75\%/25\%$ split of the tiles.

The tiles themselves are generated following [Khened et al., 2021] with median filtering and Otsu's thresholding of the HSV saturation component of the WSI image, followed by finally applying opening and closing dilation. After that, tiles of the size 256×256 are extracted. The tumor regions on the slide are indicated by polygonal annotations. The annotations are used to compute the tumor coverage per tile. Tiles with more than 25% tumor coverage are counted as tumor tiles and all tiles with 0% tumor coverage are counted as non-tumor tiles. Tumor tiles with less than 25%

coverage by the tumor annotation are excluded from our standard training, to minimize the risk of label noise that could arise due to high inter-observer variability [Jensen et al., 2019, Joskowicz et al., 2019, Karimi et al., 2020].

TCGA: In the slide-level analysis, we utilize tissue slides of colorectal cancer (CRC) from TCGA to predict the MSI status, following the approach described in [Kather et al., 2019, Bilal et al., 2021]. Following the procedure outlined in [Kather et al., 2019], we include only slides labeled as MSI-H and MSS, excluding slides with interfering markers or missing resolution information. This yields a total of 322 slides available for training and testing, comprising 59 MSI-labeled slides and 263 MSS-labeled slides. For the test set we define a domain shift by location, by allocating the 60 slides from the submitting centers MSKCC and Roswell Park for testing.

3.2 Training setup and hyperparameter tuning

For our tile-level experiments, we use a ResNet-34 [He et al., 2016] with a batch size of 128 and a learning rate of 0.001 for all our experiments. As the optimizer, we utilize Adam [Kingma and Ba, 2017], with a reduction of the learning rate by a factor of 10 if the validation loss, which is chosen as the cross-entropy loss, does not decrease for 3 epochs. For data augmentations, we follow [Tellez et al., 2019] applying random crops to size 224×224, random $90°$ rotations and color jitter (brightness:$\pm 20\%$, contrast:$\pm 30\%$, hue:$\pm 10\%$, saturation:$\pm 10\%$). The inputs are normalized with the mean and variance of the training data. The best model is chosen by accuracy on the validation set. During training, we balance the training set by samples per class, but we do not balance the validation set, as we want to evaluate our methods on all available data.

For the Deep Ensemble architecture, we choose $n = 5$ members following recent literature [Linmans et al., 2020, Thagaard et al., 2020]. For MCDO, we place a dropout layer after each ResNet block, with a dropout probability $p = 0.3$. This is in contrast to [Linmans et al., 2020, Thagaard et al., 2020], who only place a dropout layer before the last layer, observing no improvement in performance. For inference during testing, we use 10 SVI-, MCDO- and TTA-samples. Following [Wenzel et al., 2020], we use an additional hyperparameter for weighting the influence of the SVI prior (Kullback-Leibler-Divergence to the normal distribution) on the training. We tune this hyperparameter as well as the dropout probability, the dropout layer placement and the learning rate with the python library Optuna [Akiba et al., 2019].

For the slide-level experiments, we use the open-source CLAM method [Lu et al., 2021]. The CLAM pipeline consists of two central elements: First, tile-level features are extracted using a ResNet-18 [He et al., 2016] pretrained on ImageNet [Deng et al., 2009], such that each slide is represented as a bag of tile-level features. In the second step, an attention-based mechanism [Ilse et al., 2018] is applied to compute a slide-level prediction. For training the approach, we use the same setup as described in [Lu et al., 2021], by combining the slide-level cross-entropy loss with a tile-level SVM clustering loss. After extracting the test slides, we use 80% of the remaining slides for training and 20% for validation. We make sure that both labels MSI and MSS are distributed equally between all splits and use weighted sampling of both classes for training. We set the initial learning rate to 2^{-4}, monitor the validation loss with early stopping and set a minimum amount of 50 and maximum amount of 200 training epochs. The method is trained with dropout probability set to $p = 0.25$. For our uncertainty evaluations, we train Deep Ensembles with $n = 5$ members and for MCDO we use 10 runs at inference.

All our experiments are conducted with PyTorch 1.11 on Nvidia GPUs with CUDA 11.3.

4 Results

We trained each method 5 times with different seeds, reporting their average or median performance.

4.1 Reject Option

We compare the uncertainty methods in terms of their ability to detect mispredictions. For that, we compute the (Balanced) Accuracy-Reject Curves (see Section 2.3). In Figure 1, we compare the methods and their performance with an increasing ratio of rejected tiles, for the test slides on the ID centers and OOD centers on the weak and strong domain shift, respectively. To determine the most uncertain tiles that are rejected, we use the confidence measure. On the ID centers of the weak shift setup, all methods perform similarly well, with the exception being the TTA Ensemble, which starts with higher balanced accuracy, but is the only method that does not show a monotonic increase of balanced accuracy with a growing rejection rate. A similar trend can be observed on the OOD centers, where TTA shows stagnating performance after rejecting more than 50% of uncertain tiles.

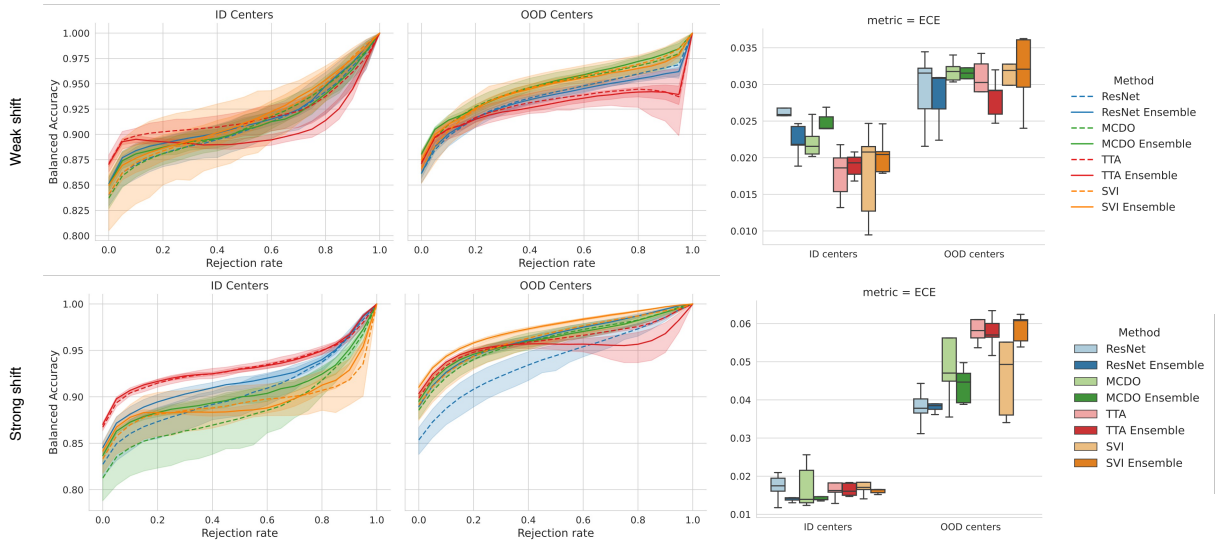


Figure 1: (Balanced) Accuracy-Reject Curves on ID and OOD centers, as well as the calibration error, for the weak and strong domain shift setup. The x-axis contains the proportion of rejected inputs over the dataset, which is plotted against the reached Balanced Accuracy on the remaining images. The order of the excluded points was determined by the predictive confidence (see B). We plot the mean curves over all 5 trials, with the shaded area denoting the 95% confidence interval. In the plots on the right side, we compare the influence of the uncertainty estimation methods on network calibration in terms of median ECE over all slides of the test sets, on both ID and OOD centers.

Table 1: Mean and standard deviation of the area under the curve of the accuracy-reject curves ($AUARC$) presented in Figure 1.

Shift	Method	ID Centers	OOD Centers
Weak	ResNet	$0.9105_{\pm 0.0190}$	$0.9375_{\pm 0.0094}$
	ResNet Ensemble	$0.9169_{\pm 0.0071}$	$0.9354_{\pm 0.0044}$
	MCDO	$0.9124_{\pm 0.0134}$	$0.9470_{\pm 0.0112}$
	MCDO Ensemble	$0.9126_{\pm 0.0104}$	$\mathbf{0.9494}_{\pm 0.0034}$
	TTA	$\mathbf{0.9200}_{\pm 0.0140}$	$0.9305_{\pm 0.0169}$
	TTA Ensemble	$0.9051_{\pm 0.0053}$	$0.9283_{\pm 0.0056}$
	SVI	$0.9156_{\pm 0.0329}$	$0.9467_{\pm 0.0148}$
	SVI Ensemble	$0.9183_{\pm 0.0133}$	$0.9459_{\pm 0.0051}$
Strong	ResNet	$0.9057_{\pm 0.0169}$	$0.9402_{\pm 0.0150}$
	ResNet Ensemble	$0.9184_{\pm 0.0070}$	$0.9639_{\pm 0.0043}$
	MCDO	$0.8864_{\pm 0.0303}$	$0.9609_{\pm 0.0093}$
	MCDO Ensemble	$0.9048_{\pm 0.0075}$	$0.9625_{\pm 0.0070}$
	TTA	$0.9321_{\pm 0.0047}$	$0.9607_{\pm 0.0024}$
	TTA Ensemble	$\mathbf{0.9332}_{\pm 0.0024}$	$0.9547_{\pm 0.0095}$
	SVI	$0.8948_{\pm 0.0269}$	$0.9643_{\pm 0.0110}$
	SVI Ensemble	$0.8958_{\pm 0.0058}$	$\mathbf{0.9739}_{\pm 0.0015}$

In contrast, within the strong shift setup, TTA and TTA Ensemble achieve the highest balanced accuracies along the entire curve on the ID centers, while the MCDO and SVI methods perform worst. On the OOD centers the ranking is mostly reversed, with the SVI Ensemble leading to the highest accuracy-reject-curves, while the baseline ResNet and the TTA methods perform worst. Surprisingly, the Balanced Accuracy values on the OOD centers are partially higher than on the ID centers. In A, we elaborate on this behavior on the OOD data. Additionally, we evaluate and compare the classification performance of these methods using the median balanced accuracy over all slides of the test datasets.

In Table 1 we show the area under the curve for the accuracy-reject curves ($AUARC$) for the weak and strong domain shift scenarios. For the ID centers of the weak domain shift, all methods but TTA Ensemble improve upon the $AUARC$ compared to the baseline ResNet, with TTA, SVI Ensemble and ResNet Ensemble performing the best. On the in-distribution data of the strong shift, however, all SVI and MCDO methods perform worse or are comparable to the

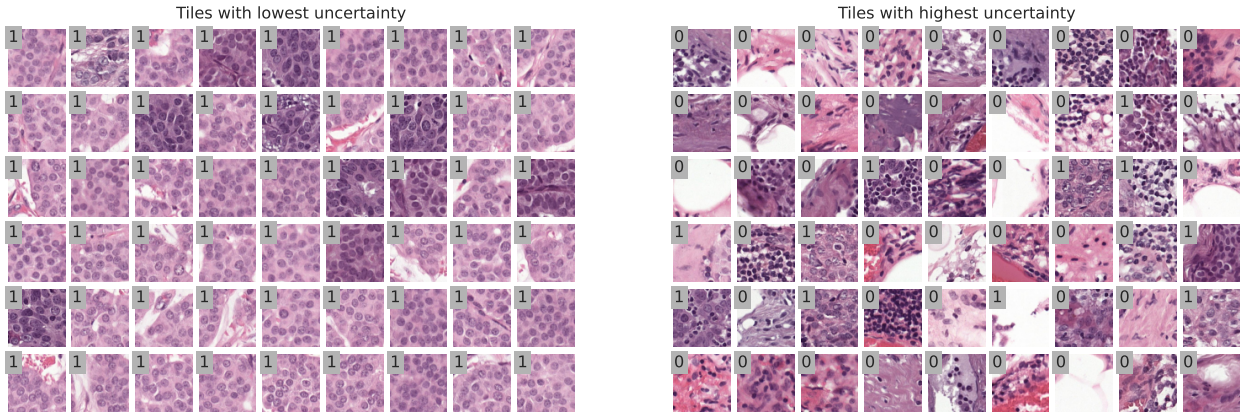


Figure 2: Least and most uncertain tiles from the in-distribution test set computed by the confidence of a ResNet Ensemble. The numbers represent the ground-truth labels: '1' indicates tumor and '0' indicates a non-tumor tile.

ResNet baseline. Here both TTA approaches and the ResNet Ensemble are the only methods to substantially improve upon the ResNet baseline. By using the $AUARC$ metric, we can identify the MCDO Ensemble as best performing method on the OOD centers of the weak shift setup and the SVI Ensemble as best performing method on the OOD centers of the strong shift setup, while the TTA methods underperform on the OOD data of the weak shift. On the OOD data of the strong shift, every method improves upon the baseline.

From our experiments, no single method can be identified, that performs best between all data splits, as the rankings of the methods vary heavily between the ID and OOD data, as well as between the weak shift and strong shift setup. However, ensemble approaches often outperformed their singular counterparts under the domain shift scenarios. Further analysis of the ranking of the uncertainty methods in a leave-one-out setup by centers, which comes to the same conclusion, can be found in C.

In Figure 2 we present a collection of the most certain and most uncertain tiles within the ID test data of the strong shift setup, computed with a ResNet Ensemble. We observe that the neural network appears to be most confident on tumor tiles (label 1), that cover the whole tile and possess a similar cell structure. For the most uncertain tiles on the right side, no comparable structure among the tiles is observable. These tiles both contain tumor and non-tumor tissue and often lie at border regions between different tissue types. Many uncertain tiles seem to lie at the border of annotated tumor regions, that we suspect to have a larger degree of label noise and are harder to distinguish due to features that are present in both healthy and tumorous tissue.

4.2 Calibration

In the plot on the right-hand side of Figure 1, we evaluate model calibration in terms of ECE (see Section 2.3) for the weak and strong shift. The ECE values have been computed as the median calibration error over all slides, as explained in A. On the ID centers in the weak shift setup, the TTA and SVI methods perform particularly well. On the ID centers for the strong shift setup, the best-performing methods are the ResNet Ensemble and MCDO Ensemble, while the TTA and SVI methods perform worse.

Under distribution shift, the best method is in fact the ResNet baseline method and its ensemble variant. All other methods perform worse on both weak and strong shift settings, with TTA Ensemble performing still quite well under the weak shift, but worst in the strong shift setting, along with the SVI Ensemble.

In conclusion like with other metrics presented, we cannot identify a best-performing method. Only ensembling approaches nearly consistently outperform their singular counterparts. Table 2 contains the detailed numeric results for our calibration experiments.

4.3 Label Noise

For translating our tile-level observations to slide-level, we stitch the tile-level predictions back to a tumor confidence map on slide-level that we show on the example of one Camelyon17 slide in Figure 3. When observing the generated confidence maps, we can see lower tumor confidence at the border of annotated tumor regions.

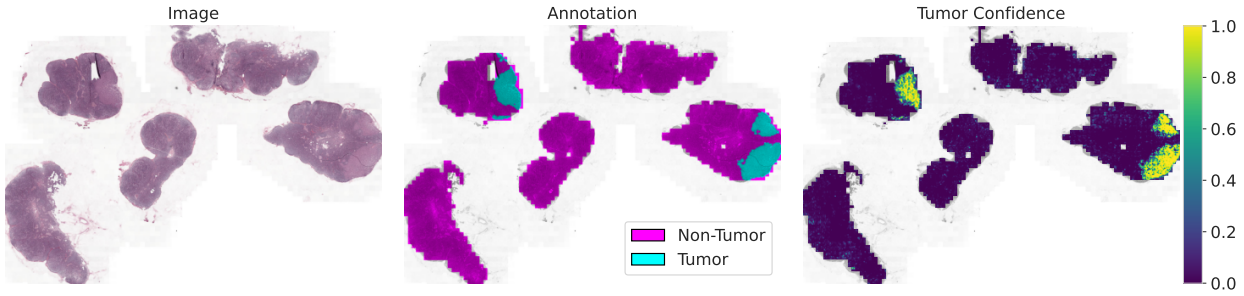


Figure 3: WSI (*patient_017_node_2*) with ground-truth annotations and model predictions. Predictions have been generated from a ResNet Ensemble. The tumor confidence decreases in areas near the border of the annotation, while the uncertainty thereby increases. This result is consistent over the whole dataset.

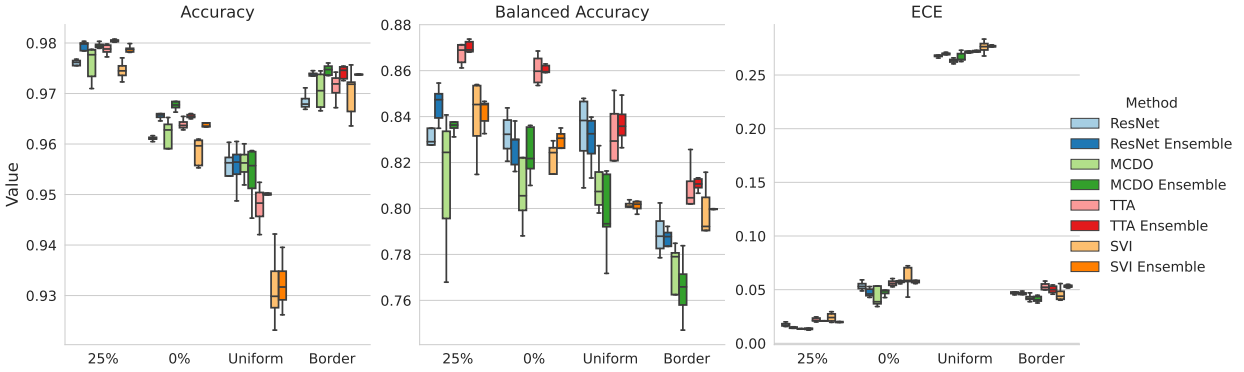


Figure 4: Performance of the proposed methods on different datasets under label noise. We compare the performance on the original dataset (25%), a dataset with a 0% tumor coverage threshold for tumor tiles (0%), applying uniform noise to the tile labels (Uniform) and randomly flipping labels of tiles which are located at the border of the annotation (Border).

Building on these observations, in our label noise experiments, we investigate the effects of imprecise tumor annotations in the border area of annotated tumor regions. To this end, we define three supplementary training datasets building on the in-distribution Camelyon17 dataset of the strong shift scenario by introducing different types of label noise to the annotations. We first create a dataset by setting the inclusion threshold by tumor coverage for tumor tiles to 0%. We previously excluded every tile that was covered by less than 25% by tumor annotations (see Section 3.1) to reduce the chance of label noise. The other two datasets are created by applying random label noise to the training split of the 0% threshold dataset. First, we apply uniform label noise to the whole slide, with a 25% chance of flipping the tile class. As this type of annotation noise does not reflect real-world inter-observer variability, we next apply label flipping to the border regions of the annotation. We flip the labels of the tumor tiles, which lie at the border of the annotation polygon and thereby are not fully covered by annotated tumor cells. We set the chance of this event occurring to 25% per tile.

In Figure 4 we show the results of the label noise experiments. Detailed results can be found in Table 3. All methods were trained on the noisy datasets but evaluated on the original test dataset. In terms of accuracy, the ensemble methods outperform their non-ensemble counterparts by a significant margin. Only on the Uniform dataset, ResNet and MCDO perform similarly to their ensemble counterparts ($\sim 95.6\%$ accuracy for each method). When viewing the balanced accuracy metric, TTA and TTA Ensemble exceed every other method by a large margin. Ensemble methods again consistently outperform their singular counterparts. The MCDO and SVI methods are the least robust methods when exposed to label noise, often performing worse than the single ResNet baseline.

We can conclude that ensembling approaches are not only more robust to domain shifts and image corruptions [Ovadia et al., 2019] but in a similar manner also to label noise, in our case in histopathological images. From our experiments, SVI and MCDO, however, are not fit to deal with label noise often leading to only slightly improved or even worse results.

TTA however does not perform well in terms of calibration error. Here MCDO outperforms TTA and SVI, which produced the overall worst calibrated predictions, in contrast to recent literature [Ashukha et al., 2020, Ayhan et al.,

2020]. We can see a large increase in ECE on the dataset with uniform label noise and a slight increase in the miscalibration on the other two datasets with label noise compared to our baseline dataset. Except for the original dataset, no trend of ensembling methods decreasing calibration error is visible. Ensembling does not seem to improve calibration when confronted with larger quantities of label noise, contrary to the setting of domain shift (Figure 1) where ensembling decreased the calibration error.

4.4 Slide-level Analysis

For the slide-level analysis, we aim to predict the MSI status on WSIs of colorectal cancer tissue from the TCGA dataset as described in Section 3.1. Since we evaluated the performance of common uncertainty methods on the tile-level before, we first try to infer a slide-level prediction by using tile-level uncertainties. A similar approach has been presented in the concurrent work by [Linmans et al., 2023] for the slide-level prediction of prostate cancer. To train the tile-level approach, at first we use a subtyper network to identify tumor tiles on each WSI. We then assign the binary slide-level label (MSS or MSI) to each tumor tile of the corresponding WSI and train an ensemble of five ResNet-34, comparable to the previous tile-level evaluations. To compute a slide-level prediction, we average the predictions of the top 1% most confident tile-level scores. By evaluating five different runs using the described method, we retrieve AUROC values with mean and standard deviation 0.6243 ± 0.0610 on the test set.

Besides aggregating tile-level predictions, there exist more sophisticated methods in the context of WSI classification, one of which is the CLAM method [Lu et al., 2021]. We trained and evaluated the CLAM method on the same data splits and the AUROC values over 5 runs are 0.7168 ± 0.0328. The significant increase in performance leads to the conclusion that the attention-based CLAM approach is better suited for the slide-level prediction task than aggregating tile-level predictions by uncertainty.

Following our tile-level experiments, we evaluate the ability for selective classification on the slide-level under domain shift. For this, we implemented Deep Ensembles and Monte-Carlo Dropout on top of the better performing CLAM-method. In Figure 5 we show the Accuracy-Reject curves for the slide-level prediction tasks. From the curves, we can see that rejecting slides by uncertainty leads to improvements in performance, comparable to the tile-level experiments. We also observe a similar trend as in the tile-level evaluations, that ensembles of methods perform better than their single model counterparts.

Overall, we can conclude that rejecting slide-level predictions by uncertainty is a viable approach to selective classification and can significantly increase predictive accuracy.

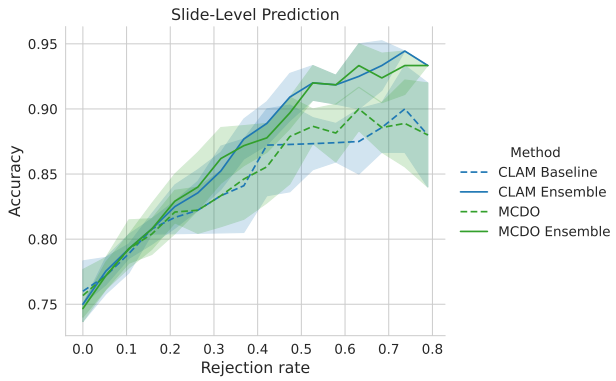


Figure 5: Accuracy-Reject Curves for slide-level MSI prediction using the CLAM method [Lu et al., 2021]

5 Discussion

In the previous section, we have gone through an extensive comparison of the most prominent methods for uncertainty estimation under domain shift on histopathological WSIs. In this section, we want to discuss the observations that we have made and we want to formulate recommendations for other researchers that try to integrate uncertainty estimation into digital pathology.

Our results show that mispredictions can be detected reliably and that the right methods can increase the robustness to domain shift and label noise, while also providing better-calibrated predictions.

Among the methods for uncertainty estimation, ensembles lead to the most reliable uncertainty estimates and additionally improve classification performance and network calibration. As expected, combining MCDO, TTA and SVI with ensembling can lead to further improvements in classification performance, however, it also entails a steep increase in computational requirements, which might not be possible in some medical environments. In the case of MCDO and SVI, architectural changes in the neural network need to be made and these methods performed the most inconsistent across our experiments. As the rankings of all investigated methods varied heavily between different settings, see also C, no best method can be identified for all tasks.

In terms of misprediction detection on ID data, all methods provide a reliable improvement in classification performance, with a growing rejection rate making misprediction detection a feasible scenario in a clinical setting. The TTA methods performed the most inconsistent for selective classification, as they were the only methods with a non-monotonic increase of the accuracy-reject curves. The largest increase for every method is at the beginning of the accuracy-reject-curve, with the slope often decreasing notably around the 20% reject rate threshold. From our results, it is plausible that in many cases it could be enough to only reject around 20% of most uncertain predictions to receive a significant accuracy boost.

We could observe a strong increase in calibration error from the ID centers to the OOD centers. However, from our experiments, no single non-ensemble method outperformed the other approaches over all domain shifts and data splits in terms of calibration error. Ensembles often improved the measured calibration.

By sorting the tile predictions by uncertainty, we observe visually recognizable differences between the most certain and most uncertain tiles, which are consistent with all methods. On the WSIs, the networks make especially confident predictions for tiles that lie inside tumor metastases, while being the most uncertain at the border of tumor regions, which can also be seen when visualizing the uncertainty on the slide-level. In our label noise experiments, we could immediately see the impact of including tissue-border tiles with noisy labels, with a drop in classifier performance. Care should therefore be taken in the correct preparation of the training data, as inaccurate annotations or label noise induced by the tiling process in the border regions can significantly impact performance. In our experiments, the ensemble approaches and TTA showed increased resistance to label noise.

Besides analyzing the influence of uncertainty estimation methods on the tile-level tumor prediction task, we have also applied uncertainty estimation to the slide-level task of MSI prediction on slides of colorectal cancer tissue. Since clinical diagnoses are performed on slide-level, it is an important insight that with the help of uncertainty estimation, mispredictions can be identified on slide-level and the performance of the neural network can be improved. Here ensembles again performed better than their singular counterparts, while MCDO did not improve upon the baseline CLAM method.

The correct choice of metrics is an important consideration when dealing with histopathological data. In our experiments, we noticed that different splits of the dataset can lead to considerably different results, see C. Evaluation therefore requires robust metrics. In our tile-level experiments we chose to use the median performance of the metric over all slides in the test dataset which proved to be more robust, see A.

6 Conclusion

Deployment of AI-based diagnostic systems in the safety-critical area of histopathology demand uncertainty-aware machine learning algorithms, which generate trust in the model's predictions.

To this end, we compared multiple uncertainty estimation methods and uncertainty metrics across domain shift and label noise scenarios in their performance, calibration and ability to detect mispredictions in the histopathological setting on tile- and slide-level. Our results show that all investigated methods are well-capable to detect mispredictions and reject inputs they are unlikely to classify correctly, which is of high clinical relevance for the reliable and safe deployment of machine learning systems. In our experiments TTA is the only method that does not lead to a monotonic increase in performance with a growing ratio of rejected inputs. Furthermore, ensembling approaches improve the calibration on histopathological data over their singular counterparts on ID and OOD data, while on the other hand, none of the included robustness and uncertainty estimation methods from the classic computer vision literature could reliably improve the calibration under domain shift.

Label noise can have a substantial effect on the quality of the predictions. As label noise can be a common problem in medical data, great care should be put into identifying potentially mislabeled inputs and in choosing data preparation techniques that produce well-labeled data points. In terms of robustness to label noise, ensembles and TTA approaches performed best in our experiments, while no method proved robust to the strong drop in calibration under label noise.

In general, ensemble approaches performed the most consistent over all our experiments. Contrary to results in the classical computer vision literature MCDO and SVI often only performed on par or slightly better than the baseline ResNet on most measures, but require substantially more computational resources during inference and architectural changes to the neural network architecture. TTA produced the best classification results on ID data, however, this advantage did not carry over under our domain shift scenarios. Additionally, it produced the worst-behaved accuracy-reject curves for the selective classification task. Overall, the ranking between the methods is inconsistent and we can not recommend one singular best-performing approach for all scenarios. As ensembling approaches lead to relatively consistent improvements over their singular counterparts they can from our experience be recommended, while also being comparatively easy to implement and use in practice.

While no single benchmark can give all-encompassing results and insights, we hope that our evaluation gives guidance for the utilization of uncertainty methods in the area of histopathology. Our published code is designed to be easily reproducible and extendable to further studies.

Acknowledgments

The research is funded by the *Ministerium für Soziales und Integration*, Baden Württemberg, Germany.

References

Andre Esteva, Brett Kuprel, Roberto A. Novoa, Justin Ko, Susan M. Swetter, Helen M. Blau, and Sebastian Thrun. Dermatologist-level classification of skin cancer with deep neural networks. *Nature*, 542(7639):115–118, February 2017. ISSN 1476-4687. doi:10.1038/nature21056.

H. A. Haenssle, C. Fink, R. Schneiderbauer, F. Toberer, T. Buhl, A. Blum, A. Kalloo, A. Ben Hadj Hassen, L. Thomas, A. Enk, L. Uhlmann, Reader study level-I and level-II Groups, Christina Alt, Monika Arenbergerova, Renato Bakos, Anne Baltzer, Ines Bertlich, Andreas Blum, Therezia Bokor-Billmann, Jonathan Bowling, Naira Braghiroli, Ralph Braun, Kristina Buder-Bakhaya, Timo Buhl, Horacio Cabo, Leo Cabrijan, Naciye Cevic, Anna Classen, David Deltgen, Christine Fink, Ivelina Georgieva, Lara-Elena Hakim-Meibodi, Susanne Hanner, Franziska Hartmann, Julia Hartmann, Georg Haus, Elti Hoxha, Raimonds Karls, Hiroshi Koga, Jürgen Kreusch, Aimilios Lallas, Pawel Majenka, Ash Marghoob, Cesare Massone, Lali Mekokishvili, Dominik Mestel, Volker Meyer, Anna Neuberger, Kari Nielsen, Margaret Oliviero, Riccardo Pampena, John Paoli, Erika Pawlik, Barbar Rao, Adriana Rendon, Teresa Russo, Ahmed Sadek, Kinga Samhaber, Roland Schneiderbauer, Anissa Schweizer, Ferdinand Toberer, Lukas Trennheuser, Lyobomira Vlahova, Alexander Wald, Julia Winkler, Priscila Wölbing, and Iris Zalaudek. Man against machine: Diagnostic performance of a deep learning convolutional neural network for dermoscopic melanoma recognition in comparison to 58 dermatologists. *Annals of Oncology: Official Journal of the European Society for Medical Oncology*, 29(8):1836–1842, August 2018. ISSN 1569-8041. doi:10.1093/annonc/mdy166.

Achim Hekler, Jochen S. Utikal, Alexander H. Enk, Axel Hauschild, Michael Weichenthal, Roman C. Maron, Carola Berking, Sebastian Haferkamp, Joachim Klode, Dirk Schadendorf, Bastian Schilling, Tim Holland-Letz, Benjamin Izar, Christof von Kalle, Stefan Fröhling, Titus J. Brinker, Laurenz Schmitt, Wiebke K. Peitsch, Friederike Hoffmann, Jürgen C. Becker, Christina Drusio, Philipp Jansen, Joachim Klode, Georg Lodde, Stefanie Sammet, Dirk Schadendorf, Wiebke Sondermann, Selma Ugurel, Jeannine Zader, Alexander Enk, Martin Salzmann, Sarah Schäfer, Knut Schäkel, Julia Winkler, Priscilla Wölbing, Hiba Asper, Ann-Sophie Bohne, Victoria Brown, Bianca Burba, Sophia Deffaa, Cecilia Dietrich, Matthias Dietrich, Katharina Antonia Drerup, Friederike Egberts, Anna-Sophie Erkens, Salim Greven, Viola Harde, Marion Jost, Merit Kaeding, Katharina Kosova, Stephan Lischner, Maria Maagk, Anna Laetitia Messinger, Malte Metzner, Rogina Motamedi, Ann-Christine Rosenthal, Ulrich Seidl, Jana Stemmermann, Kaspar Torz, Juliana Giraldo Velez, Jennifer Haiduk, Mareike Alter, Claudia Bär, Paul Bergenthal, Anne Gerlach, Christian Holtorf, Ante Karoglan, Sophie Kindermann, Luise Kraas, Moritz Felcht, Maria R. Gaiser, Claus-Detlev Klemke, Hjalmar Kurzen, Thomas Leibing, Verena Müller, Raphael R. Reinhard, Jochen Utikal, Franziska Winter, Carola Berking, Laurie Eicher, Daniela Hartmann, Markus Heppt, Katharina Kilian, Sebastian Krammer, Diana Lill, Anne-Charlotte Niesert, Eva Oppel, Elke Sattler, Sonja Senner, Jens Wallmichrath, Hans Wolff, Anja Gesierich, Tina Giner, Valerie Glutsch, Andreas Kerstan, Dagmar Presser, Philipp Schrüfer, Patrick Schummer, Ina Stolze, Judith Weber, Konstantin Drexler, Sebastian Haferkamp, Marion Mickler, Camila Toledo Stauner, and Alexander Thiem. Superior skin cancer classification by the combination of human and artificial intelligence. *European Journal of Cancer*, 120:114–121, October 2019. ISSN 0959-8049. doi:10.1016/j.ejca.2019.07.019.

Edmon Begoli, Tanmoy Bhattacharya, and Dimitri Kusnezov. The need for uncertainty quantification in machine-assisted medical decision making. *Nature Machine Intelligence*, 1(1):20–23, January 2019. ISSN 2522-5839. doi:10.1038/s42256-018-0004-1.

Benjamin Kompa, Jasper Snoek, and Andrew L. Beam. Second opinion needed: Communicating uncertainty in medical machine learning. *npj Digital Medicine*, 4(1):1–6, January 2021. ISSN 2398-6352. doi:10.1038/s41746-020-00367-3.

Jeroen van der Laak, Geert Litjens, and Francesco Ciompi. Deep learning in histopathology: The path to the clinic. *Nature Medicine*, 27(5):775–784, May 2021. ISSN 1546-170X. doi:10.1038/s41591-021-01343-4.

Chuan Guo, Geoff Pleiss, Yu Sun, and Kilian Q. Weinberger. On Calibration of Modern Neural Networks. In *Proceedings of the 34th International Conference on Machine Learning*, pages 1321–1330. PMLR, July 2017.

Neil Band, Tim G J Rudner, Qixuan Feng, Angelos Filos, Zachary Nado, Michael W Dusenberry, Ghassen Jerfel, Dustin Tran, and Yarin Gal. Benchmarking Bayesian Deep Learning on Diabetic Retinopathy Detection Tasks. In *NeurIPS 2021*, page 15, 2021.

Paul F. Jaeger, Carsten Tim Lüth, Lukas Klein, and Till J. Bungert. A Call to Reflect on Evaluation Practices for Failure Detection in Image Classification. In *ICLR 2023*, February 2023.

Dan Hendrycks and Thomas Dietterich. Benchmarking Neural Network Robustness to Common Corruptions and Perturbations. In *ICLR 2019*, page 16, 2019.

Yaniv Ovadia, Emily Fertig, Jie Ren, Zachary Nado, D. Sculley, Sebastian Nowozin, Joshua Dillon, Balaji Lakshminarayanan, and Jasper Snoek. Can you trust your model' s uncertainty? Evaluating predictive uncertainty under dataset shift. In *Advances in Neural Information Processing Systems*, volume 32. Curran Associates, Inc., 2019.

Karin Stacke, Gabriel Eilertsen, Jonas Unger, and Claes Lundström. Measuring Domain Shift for Deep Learning in Histopathology. *IEEE Journal of Biomedical and Health Informatics*, 25(2):325–336, February 2021. ISSN 2168-2208. doi:10.1109/JBHI.2020.3032060.

David Tellez, Geert Litjens, Péter Bándi, Wouter Bulten, John-Melle Bokhorst, Francesco Ciompi, and Jeroen van der Laak. Quantifying the effects of data augmentation and stain color normalization in convolutional neural networks for computational pathology. *Medical Image Analysis*, 58:101544, December 2019. ISSN 1361-8415. doi:10.1016/j.media.2019.101544.

Davood Karimi, Haoran Dou, Simon K. Warfield, and Ali Gholipour. Deep learning with noisy labels: Exploring techniques and remedies in medical image analysis. *Medical Image Analysis*, 65:101759, October 2020. ISSN 1361-8415. doi:10.1016/j.media.2020.101759.

Jasper Linmans, Jeroen van der Laak, and Geert Litjens. Efficient Out-of-Distribution Detection in Digital Pathology Using Multi-Head Convolutional Neural Networks. In *Proceedings of the Third Conference on Medical Imaging with Deep Learning*, pages 465–478. PMLR, September 2020.

Jeppe Thagaard, Søren Hauberg, Bert van der Vegt, Thomas Ebstrup, Johan D. Hansen, and Anders B. Dahl. Can You Trust Predictive Uncertainty Under Real Dataset Shifts in Digital Pathology? In Anne L. Martel, Purang Abolmaesumi, Danail Stoyanov, Diana Mateus, Maria A. Zuluaga, S. Kevin Zhou, Daniel Racoceanu, and Leo Joskowicz, editors, *Medical Image Computing and Computer Assisted Intervention – MICCAI 2020*, Lecture Notes in Computer Science, pages 824–833, Cham, 2020. Springer International Publishing. ISBN 978-3-030-59710-8. doi:10.1007/978-3-030-59710-8_80.

Balaji Lakshminarayanan, Alexander Pritzel, and Charles Blundell. Simple and Scalable Predictive Uncertainty Estimation using Deep Ensembles. In *Advances in Neural Information Processing Systems*, volume 30. Curran Associates, Inc., 2017.

Yarin Gal and Zoubin Ghahramani. Dropout as a Bayesian Approximation: Representing Model Uncertainty in Deep Learning. In *Proceedings of The 33rd International Conference on Machine Learning*, pages 1050–1059. PMLR, June 2016.

Jasper Linmans, Stefan Elfwing, Jeroen van der Laak, and Geert Litjens. Predictive uncertainty estimation for out-of-distribution detection in digital pathology. *Medical Image Analysis*, 83:102655, January 2023. ISSN 1361-8415. doi:10.1016/j.media.2022.102655.

Charles Blundell, Julien Cornebise, Koray Kavukcuoglu, and Daan Wierstra. Weight Uncertainty in Neural Networks. In *Proceedings of the 32nd International Conference on Machine Learning*, pages 1613–1622. PMLR, June 2015.

Murat Seçkin Ayhan and Philipp Berens. Test-time Data Augmentation for Estimation of Heteroscedastic Aleatoric Uncertainty in Deep Neural Networks. In *Proceedings of the First Conference on Medical Imaging with Deep Learning*, page 9, 2018.

Péter Bándi, Oscar Geessink, Quirine Manson, Marcory Van Dijk, Maschenka Balkenhol, Meyke Hermsen, Babak Ehteshami Bejnordi, Byungjae Lee, Kyunghyun Paeng, Aoxiao Zhong, Quanzheng Li, Farhad Ghazvinian Zanjani, Svitlana Zinger, Keisuke Fukuta, Daisuke Komura, Vlado Ovtcharov, Shenghua Cheng, Shaoqun Zeng, Jeppe Thagaard, Anders B. Dahl, Huangjing Lin, Hao Chen, Ludwig Jacobsson, Martin Hedlund, Melih Çetin, Eren Halıcı, Hunter Jackson, Richard Chen, Fabian Both, Jörg Franke, Heidi Küsters-Vandevelde, Willem Vreuls, Peter Bult, Bram van Ginneken, Jeroen van der Laak, and Geert Litjens. From Detection of Individual Metastases to Classification of Lymph Node Status at the Patient Level: The CAMELYON17 Challenge. *IEEE Transactions on Medical Imaging*, 38(2):550–560, February 2019. ISSN 1558-254X. doi:10.1109/TMI.2018.2867350.

Yang Liu, Nilay S. Sethi, Toshinori Hinoue, Barbara G. Schneider, Andrew D. Cherniack, Francisco Sanchez-Vega, Jose A. Seoane, Farshad Farshidfar, Reanne Bowlby, Mirazul Islam, Jaegil Kim, Walid Chatila, Rehan Akbani, Rupa S. Kanchi, Charles S. Rabkin, Joseph E. Willis, Kenneth K. Wang, Shannon J. McCall, Lopa Mishra, Akinyemi I. Ojesina, Susan Bullman, Chandra Sekhar Pedamallu, Alexander J. Lazar, Ryo Sakai, Samantha J. Caesar-Johnson, John A. Demchok, Ina Felau, Melpomeni Kasapi, Martin L. Ferguson, Carolyn M. Hutter, Heidi J. Sofia, Roy Tarnuzzer, Zhining Wang, Liming Yang, Jean C. Zenklusen, Jiashan (Julia) Zhang, Sudha Chudamani, Jia Liu, Laxmi Lolla, Rashi Naresh, Todd Pihl, Qiang Sun, Yunhu Wan, Ye Wu, Juok Cho, Timothy DeFreitas, Scott Frazer, Nils Gehlenborg, Gad Getz, David I. Heiman, Jaegil Kim, Michael S. Lawrence, Pei Lin, Sam Meier, Michael S. Noble, Gordon Saksena, Doug Voet, Hailei Zhang, Brady Bernard, Nyasha Chambwe, Varsha Dhankani, Theo Knijnenburg, Roger Kramer, Kalle Leinonen, Yuexin Liu, Michael Miller, Sheila Reynolds, Ilya Shmulevich, Vesteinn Thorsson, Wei Zhang, Rehan Akbani, Bradley M. Broom, Apurva M. Hegde, Zhenlin Ju, Rupa S. Kanchi, Anil Korkut, Jun Li, Han Liang, Shiyun Ling, Wenbin Liu, Yiling Lu, Gordon B. Mills, Kwok-Shing Ng, Arvind Rao, Michael Ryan, Jing Wang, John N. Weinstein, Jiexin Zhang, Adam Abeshouse, Joshua Armenia, Debyani Chakravarty, Walid K. Chatila, Inode Bruijn, Jianjiong Gao, Benjamin E. Gross, Zachary J. Heins, Ritika Kundra, Konnor La, Marc Ladanyi,

Augustin Luna, Moriah G. Nissan, Angelica Ochoa, Sarah M. Phillips, Ed Reznik, Francisco Sanchez-Vega, Chris Sander, Nikolaus Schultz, Robert Sheridan, S. Onur Sumer, Yichao Sun, Barry S. Taylor, Jioajiao Wang, Hongxin Zhang, Pavana Anur, Myron Peto, Paul Spellman, Christopher Benz, Joshua M. Stuart, Christopher K. Wong, Christina Yau, D. Neil Hayes, Joel S. Parker, Matthew D. Wilkerson, Adrian Ally, Miruna Balasundaram, Reanne Bowlby, Denise Brooks, Rebecca Carlsen, Eric Chuah, Noreen Dhalla, Robert Holt, Steven J. M. Jones, Katayoon Kasaian, Darlene Lee, Yussanne Ma, Marco A. Marra, Michael Mayo, Richard A. Moore, Andrew J. Mungall, Karen Mungall, A. Gordon Robertson, Sara Sadeghi, Jacqueline E. Schein, Payal Sipahimalani, Angela Tam, Nina Thiessen, Kane Tse, Tina Wong, Ashton C. Berger, Rameen Beroukhim, Andrew D. Cherniack, Carrie Cibulskis, Stacey B. Gabriel, Galen F. Gao, Gavin Ha, Matthew Meyerson, Steven E. Schumacher, Juliann Shih, Melanie H. Kucherlapati, Raju S. Kucherlapati, Stephen Baylin, Leslie Cope, Ludmila Danilova, Moiz S. Bootwalla, Phillip H. Lai, Dennis T. Maglinte, David J. Van Den Berg, Daniel J. Weisenberger, J. Todd Auman, Saianand Balu, Tom Bodenheimer, Cheng Fan, Katherine A. Hoadley, Alan P. Hoyle, Stuart R. Jefferys, Corbin D. Jones, Shaowu Meng, Piotr A. Mieczkowski, Lisle E. Mose, Amy H. Perou, Charles M. Perou, Jeffrey Roach, Yan Shi, Janae V. Simons, Tara Skelly, Matthew G. Soloway, Donghui Tan, Umadevi Veluvolu, Huihui Fan, Toshinori Hinoue, Peter W. Laird, Hui Shen, Wanding Zhou, Michelle Bellair, Kyle Chang, Kyle Covington, Chad J. Creighton, Huyen Dinh, HarshaVardhan Doddapaneni, Lawrence A. Donehower, Jennifer Drummond, Richard A. Gibbs, Robert Glenn, Walker Hale, Yi Han, Jianhong Hu, Viktoriya Korchina, Sandra Lee, Lora Lewis, Wei Li, Xiuping Liu, Margaret Morgan, Donna Morton, Donna Muzny, Jireh Santibanez, Margi Sheth, Eve Shinbrot, Linghua Wang, Min Wang, David A. Wheeler, Liu Xi, Fengmei Zhao, Julian Hess, Elizabeth L. Appelbaum, Matthew Bailey, Matthew G. Cordes, Li Ding, Catrina C. Fronick, Lucinda A. Fulton, Robert S. Fulton, Cyriac Kandoth, Elaine R. Mardis, Michael D. McLellan, Christopher A. Miller, Heather K. Schmidt, Richard K. Wilson, Daniel Crain, Erin Curley, Johanna Gardner, Kevin Lau, David Mallery, Scott Morris, Joseph Paulauskis, Robert Penny, Candace Shelton, Troy Shelton, Mark Sherman, Eric Thompson, Peggy Yena, Jay Bowen, Julie M. Gastier-Foster, Mark Gerken, Kristen M. Leraas, Tara M. Lichtenberg, Nilsa C. Ramirez, Lisa Wise, Erik Zmuda, Niall Corcoran, Tony Costello, Christopher Hovens, Andre L. Carvalho, Ana C. de Carvalho, José H. Fregnani, Adhemar Longatto-Filho, Rui M. Reis, Cristovam Scapulatempo-Neto, Henrique C. S. Silveira, Daniel O. Vidal, Andrew Burnette, Jennifer Eschbacher, Beth Hermes, Ardene Noss, Rosy Singh, Matthew L. Anderson, Patricia D. Castro, Michael Ittmann, David Huntsman, Bernard Kohl, Xuan Le, Richard Thorp, Chris Andry, Elizabeth R. Duffy, Vladimir Lyadov, Oxana Paklina, Galiya Setdikova, Alexey Shabunin, Mikhail Tavobilov, Christopher McPherson, Ronald Warnick, Ross Berkowitz, Daniel Cramer, Colleen Feltmate, Neil Horowitz, Adam Kibel, Michael Muto, Chandrajit P. Raut, Andrei Malykh, Jill S. Barnholtz-Sloan, Wendi Barrett, Karen Devine, Jordonna Fulop, Quinn T. Ostrom, Kristen Shimmel, Yingli Wolinsky, Andrew E. Sloan, Agostino De Rose, Felice Giuliante, Marc Goodman, Beth Y. Karlan, Curt H. Hagedorn, John Eckman, Jodi Harr, Jerome Myers, Kelinda Tucker, Leigh Anne Zach, Brenda Deyarmin, Hai Hu, Leonid Kvecher, Caroline Larson, Richard J. Mural, Stella Somiari, Ales Vicha, Tomas Zelinka, Joseph Bennett, Mary Iacocca, Brenda Rabeno, Patricia Swanson, Mathieu Latour, Louis Lacombe, Bernard Têtu, Alain Bergeron, Mary McGraw, Susan M. Staugaitis, John Chabot, Hanina Hibshoosh, Antonia Sepulveda, Tao Su, Timothy Wang, Olga Potapova, Olga Voronina, Laurence Desjardins, Odette Mariani, Sergio Roman-Roman, Xavier Sastre, Marc-Henri Stern, Feixiong Cheng, Sabina Signoretti, Andrew Berchuck, Darell Bigner, Eric Lipp, Jeffrey Marks, Shannon McCall, Roger McLendon, Angeles Secord, Alexis Sharp, Madhusmita Behera, Daniel J. Brat, Amy Chen, Keith Delman, Seth Force, Fadlo Khuri, Kelly Magliocca, Shishir Maithel, Jeffrey J. Olson, Taofeek Owonikoko, Alan Pickens, Suresh Ramalingam, Dong M. Shin, Gabriel Sica, Erwin G. Van Meir, Hongzheng Zhang, Wil Eijckenboom, Ad Gillis, Esther Korpershoek, Leendert Looijenga, Wolter Oosterhuis, Hans Stoop, Kim E. van Kessel, Ellen C. Zwarthoff, Chiara Calatozzolo, Lucia Cuppini, Stefania Cuzzubbo, Francesco DiMeco, Gaetano Finocchiaro, Luca Mattei, Alessandro Perin, Bianca Pollo, Chu Chen, John Houck, Pawadee Lohavanichbutr, Arndt Hartmann, Christine Stoehr, Robert Stoehr, Helge Taubert, Sven Wach, Bernd Wullich, Witold Kycler, Dawid Murawa, Maciej Wiznerowicz, Ki Chung, W. Jeffrey Edenfield, Julie Martin, Eric Baudin, Glenn Bubley, Raphael Bueno, Assunta De Rienzo, William G. Richards, Steven Kalkanis, Tom Mikkelsen, Houtan Noushmehr, Lisa Scarpace, Nicolas Girard, Marta Aymerich, Elias Campo, Eva Giné, Armando López Guillermo, Nguyen Van Bang, Phan Thi Hanh, Bui Duc Phu, Yufang Tang, Howard Colman, Kimberley Evason, Peter R. Dottino, John A. Martignetti, Hani Gabra, Hartmut Juhl, Teniola Akeredolu, Serghei Stepa, Dave Hoon, Keunsoo Ahn, Koo Jeong Kang, Felix Beuschlein, Anne Breggia, Michael Birrer, Debra Bell, Mitesh Borad, Alan H. Bryce, Erik Castle, Vishal Chandan, John Cheville, John A. Copland, Michael Farnell, Thomas Flotte, Nasra Giama, Thai Ho, Michael Kendrick, Jean-Pierre Kocher, Karla Kopp, Catherine Moser, David Nagorney, Daniel O'Brien, Brian Patrick O'Neill, Tushar Patel, Gloria Petersen, Florencia Que, Michael Rivera, Lewis Roberts, Robert Smallridge, Thomas Smyrk, Melissa Stanton, R. Houston Thompson, Michael Torbenson, Ju Dong Yang, Lizhi Zhang, Fadi Brimo, Jaffer A. Ajani, Ana Maria Angulo Gonzalez, Carmen Behrens, Jolanta Bondaruk, Russell Broaddus, Bogdan Czerniak, Bita Esmaeli, Junya Fujimoto, Jeffrey Gershenwald, Charles Guo, Alexander J. Lazar, Christopher Logothetis, Funda Meric-Bernstam, Cesar Moran, Lois Ramondetta, David Rice, Anil Sood, Pheroze Tamboli, Timothy Thompson, Patricia Troncoso, Anne Tsao, Ignacio Wistuba, Candace Carter, Lauren Haydu, Peter Hersey, Valerie Jakrot, Hojabr Kakavand, Richard Kefford, Kenneth Lee, Georgina Long, Graham Mann, Michael

Quinn, Robyn Saw, Richard Scolyer, Kerwin Shannon, Andrew Spillane, Jonathan Stretch, Maria Synott, John Thompson, James Wilmott, Hikmat Al-Ahmadie, Timothy A. Chan, Ronald Ghossein, Anuradha Gopalan, Douglas A. Levine, Victor Reuter, Samuel Singer, Bhuvanesh Singh, Nguyen Viet Tien, Thomas Broudy, Cyrus Mirsaidi, Praveen Nair, Paul Drwiega, Judy Miller, Jennifer Smith, Howard Zaren, Joong-Won Park, Nguyen Phi Hung, Electron Kebebew, W. Marston Linehan, Adam R. Metwalli, Karel Pacak, Peter A. Pinto, Mark Schiffman, Laura S. Schmidt, Cathy D. Vocke, Nicolas Wentzensen, Robert Worrell, Hannah Yang, Marc Moncrieff, Chandra Goparaju, Jonathan Melamed, Harvey Pass, Natalia Botnariuc, Irina Caraman, Mircea Cernat, Inga Chemencedji, Adrian Clipca, Serghei Doruc, Ghenadie Gorincioi, Sergiu Mura, Maria Pirtac, Irina Stancul, Diana Tcaciuc, Monique Albert, Iakovina Alexopoulou, Angel Arnaout, John Bartlett, Jay Engel, Sebastien Gilbert, Jeremy Parfitt, Harman Sekhon, George Thomas, Doris M. Rassl, Robert C. Rintoul, Carlo Bifulco, Raina Tamakawa, Walter Urba, Nicholas Hayward, Henri Timmers, Anna Antenucci, Francesco Facciolo, Gianluca Grazi, Mirella Marino, Roberta Merola, Ronald de Krijger, Anne-Paule Gimenez-Roqueplo, Alain Piché, Simone Chevalier, Ginette McKercher, Kivanc Birsoy, Gene Barnett, Cathy Brewer, Carol Farver, Theresa Naska, Nathan A. Pennell, Daniel Raymond, Cathy Schilero, Kathy Smolenski, Felicia Williams, Carl Morrison, Jeffrey A. Borgia, Michael J. Liptay, Mark Pool, Christopher W. Seder, Kerstin Junker, Larsson Omberg, Mikhail Dinkin, George Manikhas, Domenico Alvaro, Maria Consiglia Bragazzi, Vincenzo Cardinale, Guido Carpino, Eugenio Gaudio, David Chesla, Sandra Cottingham, Michael Dubina, Fedor Moiseenko, Renumathy Dhanasekaran, Karl-Friedrich Becker, Klaus-Peter Janssen, Julia Slotta-Huspenina, Mohamed H. Abdel-Rahman, Dina Aziz, Sue Bell, Colleen M. Cebulla, Amy Davis, Rebecca Duell, J. Bradley Elder, Joe Hilty, Bahavna Kumar, James Lang, Norman L. Lehman, Randy Mandt, Phuong Nguyen, Robert Pilarski, Karan Rai, Lynn Schoenfield, Kelly Senecal, Paul Wakely, Paul Hansen, Ronald Lechan, James Powers, Arthur Tischler, William E. Grizzle, Katherine C. Sexton, Alison Kastl, Joel Henderson, Sima Porten, Jens Waldmann, Martin Fassnacht, Sylvia L. Asa, Dirk Schadendorf, Marta Couce, Markus Graefen, Hartwig Huland, Guido Sauter, Thorsten Schlomm, Ronald Simon, Pierre Tennstedt, Oluwole Olabode, Mark Nelson, Oliver Bathe, Peter R. Carroll, June M. Chan, Philip Disaia, Pat Glenn, Robin K. Kelley, Charles N. Landen, Joanna Phillips, Michael Prados, Jeffry Simko, Karen Smith-McCune, Scott VandenBerg, Kevin Roggin, Ashley Fehrenbach, Ady Kendler, Suzanne Sifri, Ruth Steele, Antonio Jimeno, Francis Carey, Ian Forgie, Massimo Mannelli, Michael Carney, Brenda Hernandez, Benito Campos, Christel Herold-Mende, Christin Jungk, Andreas Unterberg, Andreas von Deimling, Aaron Bossler, Joseph Galbraith, Laura Jacobus, Michael Knudson, Tina Knutson, Deqin Ma, Mohammed Milhem, Rita Sigmund, Andrew K. Godwin, Rashna Madan, Howard G. Rosenthal, Clement Adebamowo, Sally N. Adebamowo, Alex Boussioutas, David Beer, Thomas Giordano, Anne-Marie Mes-Masson, Fred Saad, Therese Bocklage, Lisa Landrum, Robert Mannel, Kathleen Moore, Katherine Moxley, Russel Postier, Joan Walker, Rosemary Zuna, Michael Feldman, Federico Valdivieso, Rajiv Dhir, James Luketich, Edna M. Mora Pinero, Mario Quintero-Aguilo, Carlos Gilberto Carlotti, Jose Sebastião Dos Santos, Rafael Kemp, Ajith Sankarankuty, Daniela Tirapelli, James Catto, Kathy Agnew, Elizabeth Swisher, Jenette Creaney, Bruce Robinson, Carl Simon Shelley, Eryn M. Godwin, Sara Kendall, Cassaundra Shipman, Carol Bradford, Thomas Carey, Andrea Haddad, Jeffey Moyer, Lisa Peterson, Mark Prince, Laura Rozek, Gregory Wolf, Rayleen Bowman, Kwun M. Fong, Ian Yang, Robert Korst, W. Kimryn Rathmell, J. Leigh Fantacone-Campbell, Jeffrey A. Hooke, Albert J. Kovatich, Craig D. Shriver, John DiPersio, Bettina Drake, Ramaswamy Govindan, Sharon Heath, Timothy Ley, Brian Van Tine, Peter Westervelt, Mark A. Rubin, Jung Il Lee, Natália D. Aredes, Armaz Mariamidze, Vésteinn Thorsson, Adam J. Bass, and Peter W. Laird. Comparative Molecular Analysis of Gastrointestinal Adenocarcinomas. *Cancer Cell*, 33(4):721–735.e8, April 2018. ISSN 1535-6108. doi:10.1016/j.ccell.2018.03.010.

Alex Graves. Practical Variational Inference for Neural Networks. In *Advances in Neural Information Processing Systems*, volume 24. Curran Associates, Inc., 2011.

David M. Blei, Alp Kucukelbir, and Jon D. McAuliffe. Variational Inference: A Review for Statisticians. *Journal of the American Statistical Association*, 112(518):859–877, April 2017. ISSN 0162-1459. doi:10.1080/01621459.2017.1285773.

Yeming Wen, Paul Vicol, Jimmy Ba, Dustin Tran, and Roger Grosse. Flipout: Efficient Pseudo-Independent Weight Perturbations on Mini-Batches. In *ICLR 2018*, 2018.

Arsenii Ashukha, Dmitry Molchanov, Alexander Lyzhov, and Dmitry Vetrov. Pitfalls of In-Domain Uncertainty Estimation and Ensembling in Deep Learning. In *ICLR 2020*, page 30, 2020.

Aryan Mobiny, Aditi Singh, and Hien Van Nguyen. Risk-Aware Machine Learning Classifier for Skin Lesion Diagnosis. *Journal of Clinical Medicine*, 8(8):1241, August 2019. ISSN 2077-0383. doi:10.3390/jcm8081241.

Tanya Nair, Doina Precup, Douglas L. Arnold, and Tal Arbel. Exploring uncertainty measures in deep networks for Multiple sclerosis lesion detection and segmentation. *Medical Image Analysis*, 59:101557, January 2020. ISSN 1361-8415. doi:10.1016/j.media.2019.101557.

Christian Leibig, Vaneeda Allken, Murat Seçkin Ayhan, Philipp Berens, and Siegfried Wahl. Leveraging uncertainty information from deep neural networks for disease detection. *Scientific Reports*, 7(1):17816, December 2017. ISSN 2045-2322. doi:10.1038/s41598-017-17876-z.

Yonatan Geifman and Ran El-Yaniv. Selective Classification for Deep Neural Networks. In *Advances in Neural Information Processing Systems*, volume 30. Curran Associates, Inc., 2017.

Malik Sajjad Ahmed Nadeem, Jean-Daniel Zucker, and Blaise Hanczar. Accuracy-Rejection Curves (ARCs) for Comparing Classification Methods with a Reject Option. In *Proceedings of the Third International Workshop on Machine Learning in Systems Biology*, pages 65–81. PMLR, March 2009.

Jeremy Nixon, Michael W Dusenberry, Linchuan Zhang, Ghassen Jerfel, and Dustin Tran. Measuring Calibration in Deep Learning. In *CVPR Workshop*, page 4, 2019.

Leo Joskowicz, D. Cohen, N. Caplan, and J. Sosna. Inter-observer variability of manual contour delineation of structures in CT. *European Radiology*, 29(3):1391–1399, March 2019. ISSN 1432-1084. doi:10.1007/s00330-018-5695-5.

Martin Holm Jensen, Dan Richter Jørgensen, Raluca Jalaboi, Mads Eiler Hansen, and Martin Aastrup Olsen. Improving Uncertainty Estimation in Convolutional Neural Networks Using Inter-rater Agreement. In Dinggang Shen, Tianming Liu, Terry M. Peters, Lawrence H. Staib, Caroline Essert, Sean Zhou, Pew-Thian Yap, and Ali Khan, editors, *Medical Image Computing and Computer Assisted Intervention – MICCAI 2019*, Lecture Notes in Computer Science, pages 540–548, Cham, 2019. Springer International Publishing. ISBN 978-3-030-32251-9. doi:10.1007/978-3-030-32251-9_59.

Mahendra Khened, Avinash Kori, Haran Rajkumar, Ganapathy Krishnamurthi, and Balaji Srinivasan. A generalized deep learning framework for whole-slide image segmentation and analysis. *Scientific Reports*, 11(1):11579, June 2021. ISSN 2045-2322. doi:10.1038/s41598-021-90444-8.

Jakob Nikolas Kather, Alexander T. Pearson, Niels Halama, Dirk Jäger, Jeremias Krause, Sven H. Loosen, Alexander Marx, Peter Boor, Frank Tacke, Ulf Peter Neumann, Heike I. Grabsch, Takaki Yoshikawa, Hermann Brenner, Jenny Chang-Claude, Michael Hoffmeister, Christian Trautwein, and Tom Luedde. Deep learning can predict microsatellite instability directly from histology in gastrointestinal cancer. *Nature Medicine*, 25(7):1054–1056, July 2019. ISSN 1546-170X. doi:10.1038/s41591-019-0462-y.

Mohsin Bilal, Shan E Ahmed Raza, Ayesha Azam, Simon Graham, Mohammad Ilyas, Ian A Cree, David Snead, Fayyaz Minhas, and Nasir M Rajpoot. Development and validation of a weakly supervised deep learning framework to predict the status of molecular pathways and key mutations in colorectal cancer from routine histology images: A retrospective study. *The Lancet Digital Health*, 3(12):e763–e772, December 2021. ISSN 2589-7500. doi:10.1016/S2589-7500(21)00180-1.

Kaiming He, Xiangyu Zhang, Shaoqing Ren, and Jian Sun. Deep Residual Learning for Image Recognition. In *2016 IEEE Conference on Computer Vision and Pattern Recognition (CVPR)*, pages 770–778, Las Vegas, NV, USA, June 2016. IEEE. ISBN 978-1-4673-8851-1. doi:10.1109/CVPR.2016.90.

Diederik P. Kingma and Jimmy Ba. Adam: A Method for Stochastic Optimization. In *ICLR 2015*. arXiv, January 2017.

Florian Wenzel, Kevin Roth, Bastiaan S. Veeling, Jakub Świątkowski, Linh Tran, Stephan Mandt, Jasper Snoek, Tim Salimans, Rodolphe Jenatton, and Sebastian Nowozin. How Good is the Bayes Posterior in Deep Neural Networks Really? In *ICML 2020*, July 2020.

Takuya Akiba, Shotaro Sano, Toshihiko Yanase, Takeru Ohta, and Masanori Koyama. Optuna: A Next-generation Hyperparameter Optimization Framework. In *Proceedings of the 25th ACM SIGKDD International Conference on Knowledge Discovery & Data Mining*, KDD '19, pages 2623–2631, New York, NY, USA, July 2019. Association for Computing Machinery. ISBN 978-1-4503-6201-6. doi:10.1145/3292500.3330701.

Ming Y. Lu, Drew F. K. Williamson, Tiffany Y. Chen, Richard J. Chen, Matteo Barbieri, and Faisal Mahmood. Data-efficient and weakly supervised computational pathology on whole-slide images. *Nature Biomedical Engineering*, 5 (6):555–570, June 2021. ISSN 2157-846X. doi:10.1038/s41551-020-00682-w.

Jia Deng, Wei Dong, Richard Socher, Li-Jia Li, Kai Li, and Li Fei-Fei. ImageNet: A large-scale hierarchical image database. In *CVPR 2009*, pages 248–255, June 2009. doi:10.1109/CVPR.2009.5206848.

Maximilian Ilse, Jakub Tomczak, and Max Welling. Attention-based Deep Multiple Instance Learning. In *Proceedings of the 35th International Conference on Machine Learning*, pages 2127–2136. PMLR, July 2018.

Murat Seçkin Ayhan, Laura Kühlewein, Gulnar Aliyeva, Werner Inhoffen, Focke Ziemssen, and Philipp Berens. Expert-validated estimation of diagnostic uncertainty for deep neural networks in diabetic retinopathy detection. *Medical Image Analysis*, 64:101724, August 2020. ISSN 1361-8415. doi:10.1016/j.media.2020.101724.

A Metric Choices and Detailed Results

In this section, we motivate the usage of our metrics and give detailed results for all our experiments.

Histopathological datasets commonly exhibit a high degree of class imbalance, with classes like healthy tissue being over-represented compared to classes like tumor tissue. As a result, commonly used metrics such as AUROC and accuracy may yield misleading results, as they are highly sensitive to class imbalances. Furthermore, there can be a significant variation in the distribution of classes from slide to slide, with one slide containing minimal tumor cells while the next slide predominantly consists of a large metastasis.

In our experiments, this is the reason why we can observe higher balanced accuracy values on the OOD centers in Figure 1. The OOD center 3 for the weak shift and 4 for the strong shift both contain slides with an unusual amount of tumor tissue, which results in many tiles, where the tumor tissue covers the whole tile, which as seen in Figure 2 are the tiles where the neural networks are the most confident in their predictions. This skew in the distribution of tumor tiles, towards tiles with 100% tumor coverage and fewer border cases, in turn, leads to higher balanced accuracy values on the OOD centers. This can also be seen in the higher $AUARC$ values on center 4 compared to center 2 under the strong shift scenario in Table 4.

Such problems make reliably estimating the performance of a classifier a difficult task, as different splits of the dataset can result in very different slides for the test dataset, which in our experiments had large impacts on the measured scores and rankings of the methods.

For this reason, we report the median of our measured metrics over all slides of the test dataset. While in our experiments there were always outlier slides where metrics performed above or below average, our approach proved to be more stable to the choice of dataset split.

However, we did not employ this approach for the accuracy-reject curves of Figure 1 and Table 1, as interpreting the median curve of multiple accuracy-reject curves can be challenging. The primary focus of this task is to examine the behavior of the measured metric curve under tile-level rejection and the relative rankings of the methods. In the following, you can find the median balanced accuracy values over all slides of the test dataset.

Table 2 shows the detailed results of the classifier performance of our Camelyon17 experiments, with the median balanced accuracy and ECE over all slides of the test dataset reported.

On the ID data under both domain shifts, we can see each ensemble method improving upon its singular counterpart with only TTA Ensemble under the weak shift being on par. However, by themselves, MCDO as well as SVI, perform worse than the ResNet baseline, while TTA slightly outperforms the baseline.

Under the weak and strong domain shifts none of the alternative non-ensemble approaches improves upon the ResNet baseline, which is contrary to other reports outside of the field of histopathology [Ovadia et al., 2019]. Most ensemble approaches however improve upon the ResNet baseline and consistently perform better than their singular counterparts.

Similar to our discussion in section 4, no best method can be deduced from our experimental results. Still, ensemble approaches outperform baseline methods and consistently can be recommended.

Table 3 shows the detailed results of our label noise experiments.

Table 2: Detailed results for tile classifier performance on Camelyon17. We report the median value over 5 runs and the interquartile range for each domain shift, data split and method. The metrics are the median performance over all slides of the test dataset.

Shift	Split	Method	Balanced Accuracy ↑	ECE ↓
Weak	ID Centers	ResNet	$0.8551_{0.0264}$	$0.0259_{0.0010}$
		ResNet Ensemble	$0.8712_{0.0014}$	$0.0218_{0.0025}$
		MCDO	$0.8542_{0.0356}$	$0.0215_{0.0024}$
		MCDO Ensemble	$0.8691_{0.0054}$	$0.0240_{0.0016}$
		TTA	$0.8689_{0.0058}$	$0.0186_{0.0046}$
		TTA Ensemble	$0.8669_{0.0022}$	$0.0193_{0.0023}$
		SVI	$0.8321_{0.0368}$	$0.0208_{0.0088}$
		SVI Ensemble	$0.8731_{0.0194}$	$0.0204_{0.0027}$
	OOD Centers	ResNet	$0.6961_{0.0245}$	$0.0315_{0.0055}$
		ResNet Ensemble	$0.6863_{0.0130}$	$0.0308_{0.0043}$
		MCDO	$0.6842_{0.0447}$	$0.0318_{0.0018}$
		MCDO Ensemble	$0.6944_{0.0109}$	$0.0315_{0.0015}$
		TTA	$0.6871_{0.0324}$	$0.0303_{0.0038}$
		TTA Ensemble	$0.7046_{0.0100}$	$0.0292_{0.0033}$
		SVI	$0.6732_{0.0346}$	$0.0319_{0.0029}$
		SVI Ensemble	$0.6860_{0.0113}$	$0.0321_{0.0065}$
Strong	ID Centers	ResNet	$0.8019_{0.0031}$	$0.0175_{0.0034}$
		ResNet Ensemble	$0.8131_{0.0014}$	$0.0142_{0.0006}$
		MCDO	$0.7952_{0.0214}$	$0.0139_{0.0085}$
		MCDO Ensemble	$0.8140_{0.0086}$	$0.0139_{0.0008}$
		TTA	$0.8105_{0.0098}$	$0.0162_{0.0024}$
		TTA Ensemble	$0.8222_{0.0080}$	$0.0161_{0.0032}$
		SVI	$0.7907_{0.0104}$	$0.0171_{0.0019}$
		SVI Ensemble	$0.8126_{0.0074}$	$0.0165_{0.0008}$
	OOD Centers	ResNet	$0.7402_{0.0735}$	$0.0378_{0.0037}$
		ResNet Ensemble	$0.7940_{0.0005}$	$0.0385_{0.0014}$
		MCDO	$0.7351_{0.0250}$	$0.0470_{0.0113}$
		MCDO Ensemble	$0.7662_{0.0095}$	$0.0447_{0.0077}$
		TTA	$0.7317_{0.0232}$	$0.0582_{0.0048}$
		TTA Ensemble	$0.7348_{0.0295}$	$0.0570_{0.0036}$
		SVI	$0.6962_{0.0554}$	$0.0493_{0.0191}$
		SVI Ensemble	$0.7486_{0.0119}$	$0.0608_{0.0056}$

Table 3: Detailed results for our experiments under label noise. We report the median and the interquartile range as shown in the boxplots.

Experiment	Method	Accuracy ↑	Balanced Accuracy ↑	ECE ↓
25%	ResNet	$0.9762_{0.0010}$	$0.8291_{0.0073}$	$0.0181_{0.0020}$
	ResNet Ensemble	$0.9798_{0.0015}$	$0.8474_{0.0105}$	$0.0145_{0.0011}$
	MCDO	$0.9777_{0.0053}$	$0.8244_{0.0380}$	$\mathbf{0.0135}_{0.0001}$
	MCDO Ensemble	$0.9794_{0.0006}$	$0.8363_{0.0026}$	$0.0137_{0.0010}$
	TTA	$0.9788_{0.0013}$	$0.8689_{0.0076}$	$0.0214_{0.0026}$
	TTA Ensemble	$\mathbf{0.9805}_{0.0003}$	$\mathbf{0.8690}_{0.0043}$	$0.0207_{0.0003}$
	SVI	$0.9745_{0.0019}$	$0.8453_{0.0219}$	$0.0240_{0.0066}$
	SVI Ensemble	$0.9787_{0.0007}$	$0.8452_{0.0076}$	$0.0196_{0.0007}$
0%	ResNet	$0.9612_{0.0004}$	$0.8323_{0.0124}$	$0.0531_{0.0046}$
	ResNet Ensemble	$0.9658_{0.0007}$	$0.8299_{0.0110}$	$0.0460_{0.0061}$
	MCDO	$0.9628_{0.0048}$	$0.8055_{0.0229}$	$\mathbf{0.0387}_{0.0165}$
	MCDO Ensemble	$\mathbf{0.9677}_{0.0012}$	$0.8217_{0.0181}$	$0.0491_{0.0030}$
	TTA	$0.9637_{0.0011}$	$\mathbf{0.8598}_{0.0105}$	$0.0558_{0.0038}$
	TTA Ensemble	$0.9654_{0.0005}$	$0.8596_{0.0029}$	$0.0570_{0.0014}$
	SVI	$0.9596_{0.0050}$	$0.8243_{0.0115}$	$0.0586_{0.0129}$
	SVI Ensemble	$0.9635_{0.0008}$	$0.8306_{0.0062}$	$0.0571_{0.0020}$
Uniform	ResNet	$0.9563_{0.0037}$	$\mathbf{0.8383}_{0.0215}$	$0.2678_{0.0012}$
	ResNet Ensemble	$0.9564_{0.0039}$	$0.8325_{0.0143}$	$0.2698_{0.0013}$
	MCDO	$0.9563_{0.0034}$	$0.8074_{0.0143}$	$\mathbf{0.2633}_{0.0024}$
	MCDO Ensemble	$\mathbf{0.9557}_{0.0073}$	$0.7934_{0.0228}$	$0.2644_{0.0057}$
	TTA	$0.9483_{0.0047}$	$0.8294_{0.0204}$	$0.2712_{0.0013}$
	TTA Ensemble	$0.9500_{0.0003}$	$0.8358_{0.0092}$	$0.2719_{0.0012}$
	SVI	$0.9299_{0.0072}$	$0.8010_{0.0014}$	$0.2765_{0.0059}$
	SVI Ensemble	$0.9317_{0.0057}$	$0.8019_{0.0030}$	$0.2770_{0.0011}$
Border	ResNet	$0.9679_{0.0016}$	$0.7879_{0.0119}$	$0.0468_{0.0015}$
	ResNet Ensemble	$0.9739_{0.0005}$	$0.7878_{0.0060}$	$0.0463_{0.0015}$
	MCDO	$0.9706_{0.0065}$	$0.7790_{0.0182}$	$0.0420_{0.0025}$
	MCDO Ensemble	$\mathbf{0.9747}_{0.0018}$	$0.7659_{0.0134}$	$\mathbf{0.0405}_{0.0042}$
	TTA	$0.9719_{0.0029}$	$0.8047_{0.0098}$	$0.0523_{0.0053}$
	TTA Ensemble	$0.9746_{0.0024}$	$\mathbf{0.8107}_{0.0038}$	$0.0500_{0.0059}$
	SVI	$0.9718_{0.0058}$	$0.7922_{0.0144}$	$0.0439_{0.0074}$
	SVI Ensemble	$0.9738_{0.0001}$	$0.7997_{0.0002}$	$0.0532_{0.0017}$

B Comparison of uncertainty metrics

We compare the most commonly used uncertainty metrics of the recent literature, namely confidence, entropy and variance in their ability to distinguish uncertain from certain predictions using the $AUARC$ metric, defined in subsection 2.3.

Confidence: A commonly used method, especially in the field of calibration [Guo et al., 2017], is to take the maximum of the softmax, which is also called the "confidence" of the prediction. The core idea is that decisions that are considered certain are far away from the decision boundary, while uncertain decisions lie close to the boundary at $1/N$, where N is the number of classes.

Entropy: Another often used metric [Mobiny et al., 2019, Band et al., 2021] is to take the entropy of the prediction as a measure of uncertainty. The entropy of the model's output probability is computed as

$$H(\mathbf{y}|\mathbf{x}, \mathcal{D}) = -\sum_{c \in \mathcal{C}} p(y = c|\mathbf{x}, \mathcal{D}) \log p(y = c|\mathbf{x}, \mathcal{D}) \tag{3}$$

Since the maximum possible entropy varies with the number of classes, we compute the normed entropy as

$$\begin{aligned} H_{\text{norm}} &= \frac{H}{H_{\max}} \\ \text{with } H_{\max} &= -\sum_{i=1}^{N} \frac{1}{N} \log\left(\frac{1}{N}\right) = \log N \end{aligned} \tag{4}$$

When using the normed entropy, the uncertainty is high when $H_{\text{norm}} \to 1$ and uncertainty is low when $H_{\text{norm}} \to 0$.

Confidence ($conf$) and entropy behave very similarly in a binary classification setting. Given two predictions y_i and y_j the following relation holds between them:

$$H(y_i) < H(y_j) \iff conf(y_i) > conf(y_j) \tag{5}$$

Variance: Since all included uncertainty estimation methods generate a distribution of predictions, the variance of the distribution can be used as a measure of uncertainty [Nair et al., 2020, Leibig et al., 2017]. If all predictors agree on a result, the variance is zero, whereas a high variance indicates high uncertainty.

In Table 4 we compare the $AUARC$ values under the strong shift scenario using the three different uncertainty metrics.

As can be seen using the confidence on average produces slightly higher $AUARC$ values, while the relative order of methods stays the same. As the confidence can additionally be used with a singular model, compared to the variance approach we recommend using the confidence as uncertainty metric.

We come to the same conclusion using the weak shift setup but omit it here for brevity. The entries for the confidence metric are the same that can be found in Table 1.

Table 4: Mean and standard deviation of the area under the curve of the accuracy-reject curves ($AUARC$) presented in Figure 1 for the strong domain shift setup. We compare the confidence / entropy of a single prediction, the confidence / entropy of the mean prediction for ensembling-like approaches and the variance over multiple predictions.

Unc. Measure	Unc. Method	ID Centers	OOD (Center 2)	OOD (Center 4)
Confidence / Entropy	ResNet	$0.906_{\pm 0.017}$	$0.893_{\pm 0.031}$	$0.954_{\pm 0.010}$
Confidence / Entropy	ResNet Ensemble	$0.918_{\pm 0.007}$	$0.932_{\pm 0.010}$	$0.972_{\pm 0.004}$
	MCDO	$0.886_{\pm 0.030}$	$0.914_{\pm 0.012}$	$0.971_{\pm 0.010}$
	MCDO Ensemble	$0.905_{\pm 0.008}$	$0.924_{\pm 0.012}$	$0.971_{\pm 0.007}$
	TTA	$0.932_{\pm 0.005}$	$0.897_{\pm 0.025}$	$0.970_{\pm 0.004}$
	TTA Ensemble	$\mathbf{0.933}_{\pm 0.002}$	$0.884_{\pm 0.044}$	$0.963_{\pm 0.009}$
	SVI	$0.895_{\pm 0.027}$	$0.931_{\pm 0.025}$	$0.972_{\pm 0.012}$
	SVI Ensemble	$0.896_{\pm 0.006}$	$\mathbf{0.949}_{\pm 0.003}$	$\mathbf{0.981}_{\pm 0.002}$
Variance	ResNet Ensemble	$0.914_{\pm 0.007}$	$0.928_{\pm 0.011}$	$0.972_{\pm 0.004}$
	MCDO	$0.877_{\pm 0.033}$	$0.911_{\pm 0.011}$	$0.968_{\pm 0.012}$
	MCDO Ensemble	$0.898_{\pm 0.010}$	$0.915_{\pm 0.011}$	$0.969_{\pm 0.008}$
	TTA	$\mathbf{0.926}_{\pm 0.005}$	$0.877_{\pm 0.031}$	$0.965_{\pm 0.005}$
	TTA Ensemble	$\mathbf{0.926}_{\pm 0.002}$	$0.861_{\pm 0.053}$	$0.959_{\pm 0.010}$
	SVI	$0.890_{\pm 0.026}$	$0.929_{\pm 0.023}$	$0.970_{\pm 0.013}$
	SVI Ensemble	$0.888_{\pm 0.007}$	$\mathbf{0.942}_{\pm 0.004}$	$\mathbf{0.981}_{\pm 0.001}$

C Ranking of methods across splits

In addition to defining the weak and strong shift split for the Camelyon17 dataset, we define a leave-one-out scenario, where we train all methods on four centers and evaluate the performance on the remaining out-of-distribution center. As the strength of the domain shift and therefore the drop in predictive performance between different splits of the centers can differ significantly, it is not possible to directly compare the resulting scores. Instead, we rank all methods for every leave-one-out experiment.

In Table 5 you can see the ranking of each method for the metrics $AUARC$, Balanced Accuracy and ECE. As can be seen when looking through the columns, no method consistently performs best, instead many methods often claim a high as well as a low rank, further strengthening our results, that there is no best method for uncertainty estimation and robustness on histopathological data.

Table 5: Ranking of the methods for the metrics $AUARC$, Balanced Accuracy and ECE, across all five splits leaving one center out as OOD data. We report the rankings on the ID and OOD data.

Split	Metric	leave out	MCDO	MCDO Ens.	ResNet	ResNet Ens.	SVI	SVI Ens.	TTA	TTA Ens.
ID Centers	AUARC	0	5	2	3	7	8	1	6	4
		1	3	7	5	6	2	8	4	1
		2	5	6	2	3	7	8	1	4
		3	5	6	2	3	8	7	1	4
		4	5	4	1	6	8	7	2	3
	Balanced Accuracy	0	5	3	6	1	8	2	7	4
		1	2	6	7	8	1	3	5	4
		2	8	4	5	2	6	7	1	3
		3	8	6	7	4	3	2	1	5
		4	5	6	3	4	8	7	1	2
	ECE	0	5	7	1	3	2	8	4	6
		1	2	6	1	3	5	7	8	4
		2	2	4	5	7	6	8	1	3
		3	5	6	1	3	7	8	2	4
		4	2	4	1	3	8	7	6	5
OOD Centers	AUARC	0	6	7	2	5	1	8	4	3
		1	4	5	3	1	2	6	8	7
		2	8	6	5	2	3	1	7	4
		3	8	6	1	4	7	3	2	5
		4	8	5	1	4	7	6	2	3
	Balanced Accuracy	0	8	4	2	6	3	5	7	1
		1	3	2	7	5	1	6	8	4
		2	8	4	3	1	2	5	6	7
		3	7	4	3	5	8	6	1	2
		4	1	7	8	6	4	2	5	3
	ECE	0	3	6	1	4	2	7	5	8
		1	2	6	3	4	1	5	8	7
		2	8	4	7	2	5	1	3	6
		3	1	4	2	3	7	8	6	5
		4	2	4	1	3	6	8	5	7